Ion-beam-induced vacuum breakdown phenomena studied by emission spectroscopy

Yayu Hao(郝亚语), Lei Chen(陈磊)†, Ao Xu(徐翱), Jialin Yang(杨佳霖), Xing Wang(王杏), Zhoushilin Ruan(阮周石林), Yuanjie Shi(石元杰), and Wei Zhong(钟伟)

Institute of Electronic Engineering, China Academy of Engineering Physics, Mianyang 621999, *China*

(Received 10 August 2025; revised manuscript received 24 November 2025; accepted manuscript online 25 November 2025)

The impact of ion beams with an energy of keV on electrodes can induce microdischarges or dielectric breakdown, constituting a primary constraint on operational stability in vacuum systems. In this paper, the phenomenon of vacuum breakdown induced by 10 keV Cu ion beam bombardment on the surface of a hydrogen-containing metal electrode is studied. Utilizing spatiotemporally resolved emission spectroscopy, we capture (i) time-gated luminescence profiles during breakdown events and (ii) spectrally resolved emission maps of the electrode interface, which reveal transient desorption dynamics and spatiotemporal evolution of ionic species. Through mechanistic interpretation of these diagnostics, we elucidate the fundamental physical processes of vacuum breakdown induced by ion beam bombardment, and provide support for further understanding of the physical mechanism of breakdown induced by ion beam bombardment.

Keywords: vacuum breakdown, ion beam, time-resolved spectroscopy

PACS: 52.80.Vp, 79.20.Rf, 78.47.D–

DOI: 10.1088/1674-1056/ae23aa **CSTR:** 32038.14.CPB.ae23aa

1. Introduction

Vacuum devices or facilities typically exhibit excellent insulation properties. However, researchers have observed that the presence of an ion beam within the vacuum environment can significantly reduce its withstand voltage.[1–3] Becker and Klingelhöfer found that hydrogen or nitrogen clusters entering the electrode gap after ionization may induce vacuum breakdown.[4] Gröbner, Calder, and Erlandsson reported that during proton beam operation in a proton intersecting storage ring, residual gas in the vacuum tube becomes ionized. These ionized gas molecules accelerate under the electric field and bombard the stainless steel vacuum tube wall, causing further gas desorption that severely limits the maximum beam intensity.[5,6] Baird *et al.* identified Pb ion beams in a low-energy antiproton ring as a cause of vacuum instability, impacting beam strength and lifetime.[7] Zhang and Ahrens demonstrated that Au ion beam loss in an alternating gradient synchrotron leads to vacuum degradation and breakdown.[8] Spiller observed significant increases in vacuum pressure during high-current beam operation in a heavy-ion synchrotron, noting that beam injection losses critically affect both the vacuum system and accelerator performance.[9] These phenomena have increasingly constrained related research efforts. Nevertheless, due to limited understanding of the underlying physical mechanisms, the primary mitigation strategy remains the minimization of gas release from vacuum chambers.[10–12]

Regarding research into physical mechanisms, Sigmund and colleagues investigated gas desorption initiated by ion bombardment.[13–15] Bourne *et al.* discussed potential mechanisms through which positive ions in vacuum gaps cause breakdown.[16] Brainard and Riedel studied the characteristics of electrode bombardment by ion beams with energies of tens of keV, finding that operational ion beams reduce the withstand voltage of vacuum gaps.[17] Zalucki and Kutzner analyzed post-arc breakdown in circuit breakers, and concluded that plasma generated by initial breakdown events accelerates toward electrodes under the recovery voltage, triggering subsequent breakdown.[18] Zhang *et al.* examined inter-electrode breakdown characteristics during ion extraction in thrusters, identifying field emission, particle collisions, gas desorption, and plasma effects as contributing factors.[19] Liu *et al.* similarly studied breakdown in thruster structures, determining that thruster ion beam current is a key initiating factor.[20] Using PIC-DSMC simulations, Xu *et al.* modeled breakdown induced by high-energy proton bombardment, establishing that secondary electron avalanche ionization of desorbed gases constitutes a critical breakdown mechanism.[21]

However, existing research on ion-beam-induced breakdown is primarily focused on phenomenological observations and qualitative explanations of device-specific failures. Dedicated experimental studies on the fundamental physical mechanisms and empirical validation of theoretical models remain insufficient.

Employing emission spectroscopy diagnostics,[22–24] this study investigates vacuum breakdown induced by Cu^+ ion beam bombardment of hydrogen-containing metal electrodes.

†Corresponding author. E-mail: chenlei@caep.cn

© 2026 Chinese Physical Society and IOP Publishing Ltd. All rights, including for text and data mining, AI training, and similar technologies, are reserved.

CPB Online In-Press

By analyzing the spatiotemporal evolution of particle emissions before and after breakdown, we elucidate key physical processes during ion-beam bombardment of the electrode, providing foundational support for a deeper mechanistic understanding.

2. Experiment setup

The experimental configuration, illustrated in Fig. 1, features a Cu^+ ion source and electrode separated by a 2 mm vacuum gap within a vacuum chamber maintained at approximately 10^{-4} Pa. A pulsed power supply delivers a quasi-rectangular current waveform (amplitude 100 A, width 10 μs) to generate Cu^+ ion beams of approximately 100 mA. The metallic housing of the ion source is biased at +10 kV DC, while the 50 mm diameter hydrogen-containing titanium electrode remains grounded.

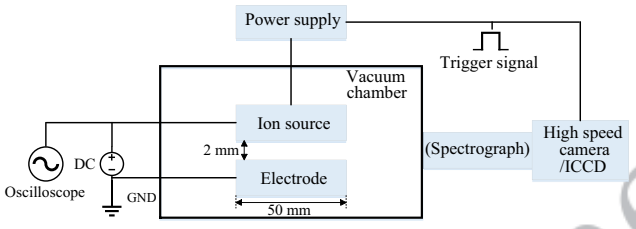


Fig. 1. Schematic diagram of the experimental setup.

The experimental diagnostics employ a sequential multimodal approach: (1) Global beam characterization: an intensified charge-coupled device (ICCD) camera captures integrated emission images throughout the duration of the ion beam. (2) Temporal resolution: a high-speed camera acquires time-resolved emission sequences. (3) Spectral analysis: spatially resolved plasma emission spectra from the electrode surface are measured using a spectrometer coupled to the high-speed camera.

3. Experimental results

3.1. Analysis of ion-beam-induced vacuum breakdown with ICCD

Within the experimental configuration illustrated in Fig. 1, diagnostic imaging was performed using an ICCD camera (20 μs exposure). Figure 2 presents the resulting vacuum gap luminescence images during ion beam bombardment of the electrode. Both panels in Fig. 2 maintain consistent orientation: the upper portion corresponds to the ion source, while the lower portion represents the titanium electrode.

When ion bombardment occurs without triggering breakdown, the luminescence exhibits a conical distribution extending from the ion source to the electrode (Fig. 2(a)). This characteristic emission pattern originates from the de-excitation of particles excited during ion source discharge. The overall luminosity remains relatively low, with localized intensification near the electrode surface attributed to collisional de-excitation of excited particles upon impact with the electrode and spatial accumulation of particles.

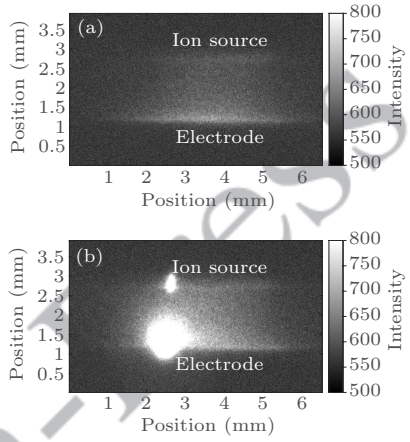


Fig. 2. The typical luminescence image of the ion beam impacting on the electrode by ICCD: (a) non-breakdown and (b) breakdown.

Upon initiation of breakdown (Fig. 2(b)), a distinct bright spherical luminous cluster emerges adjacent to the electrode surface. This high-intensity emission results from localized plasma generation during the breakdown process, where concentrated ionization produces prominent light emission confined near the electrode.

3.2. Analysis of ion-beam-induced vacuum breakdown with a high-speed camera

Since the ICCD diagnostic method captures only one luminescent image per breakdown event, a high-speed camera was employed (Fig. 1) to acquire time-continuous images and characterize the temporal evolution of the breakdown process. Figure 3 displays typical vacuum gap luminescent images before and after breakdown induced by ion beam bombardment of the hydrogen-containing titanium electrode, with each image having an exposure time of 10 ns and an inter-frame interval of 10 ns.

The breakdown time is defined as the onset of the abrupt drop in the 10 kV DC voltage (i.e., $t = 0$). A representative schematic of voltage and shutter waveforms at breakdown is presented in Fig. 4. From Fig. 3, a localized luminescent region emerges on the electrode surface 20 ns prior to breakdown, with its width increasing from 0.5 mm to 1.0 mm at breakdown. Luminescent intensity also enhances significantly, indicating that ion beam bombardment of the electrode surface initiates breakdown. Furthermore, the initial stage of surface-initiated breakdown involves a micro-discharge on the electrode, culminating in vacuum breakdown.

CPB Online In-Press

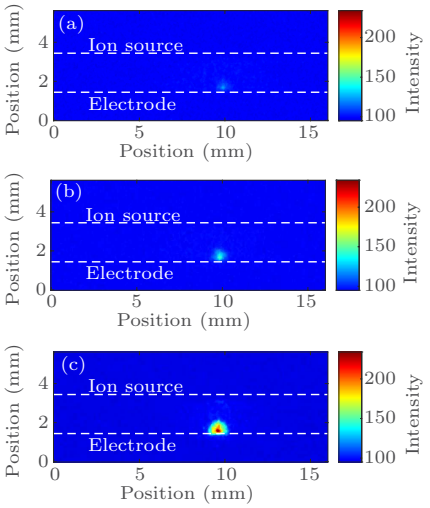


Fig. 3. Typical pre- and post-breakdown images captured by high-speed camera: (a) $t = -20$ ns, (b) $t = -10$ ns, (c) $t = 0$ ns.

To further discriminate the particle species and track their respective evolution during breakdown, optical filters centered at 656 nm and 498 nm were placed in front of the high-speed camera. These wavelengths correspond to the characteristic emission lines of H atoms and Ti atoms (the primary constituent of the electrode), respectively.

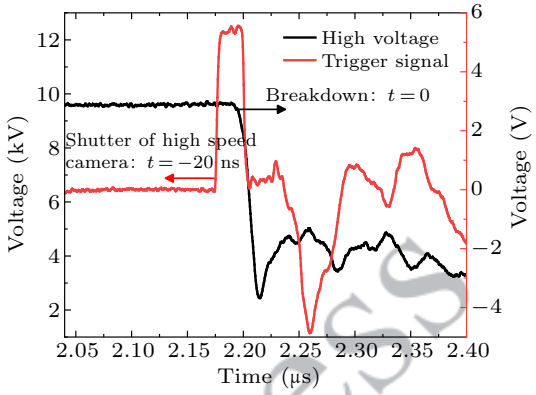


Fig. 4. Typical voltage and shutter waveform schematic diagram of breakdown.

Figures 5 and 6 present typical time-resolved luminescence images for H atoms and Ti atoms captured using the high-speed camera with the respective filters. Due to the attenuated signal intensity after filter insertion, the exposure time and inter-frame interval for these sequences were increased to 20 ns.

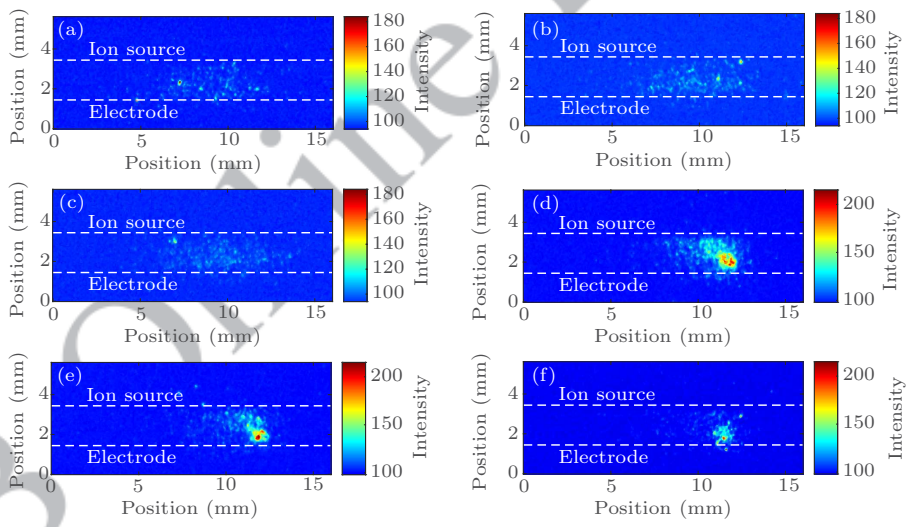


Fig. 5. Typical H atom luminescence images captured by high-speed camera: (a) $t = -75$ ns, (b) $t = -55$ ns, (c) $t = -35$ ns, (d) $t = -15$ ns, (e) $t = 5$ ns, (f) $t = 25$ ns.

From the H atom luminescence images in Fig. 5, it is observed that the emission from $t = -75$ ns to -35 ns before breakdown exhibits a relatively uniform distribution in the vacuum gap, with enhanced brightness near the electrode surface. This indicates the release of H atoms from the electrode due to Cu^+ ion bombardment. At $t = -15$ ns before breakdown, H atom luminescence in the vacuum gap increases significantly, particularly near the electrode surface, demonstrating substantial release of H atoms at this stage. Combined with Fig. 3, we can infer that Cu^+ ion bombardment releases both H atoms and secondary electrons. These electrons collide with high-density H atoms near the electrode, ionizing them to generate additional secondary electrons and H^+ ions, forming a micro-discharge on the electrode surface.

At breakdown onset, extensive ionization of H atoms near the electrode reduces luminescence intensity. Concurrently, rapid electron and positive ion multiplication leads to electron avalanche formation, culminating in breakdown.

As shown in Fig. 6, the Ti atom luminescence distribution and evolution resemble those of H atoms. However, Ti atom emission in the vacuum gap is weaker and more discretely distributed. This emission arises from radiative relaxation of excited-state Ti atoms sputtered during Cu^+ bombardment of the electrode. The lower population density of Ti species relative to H atoms prevents spatially resolved profile formation.

CPB Online In-Press

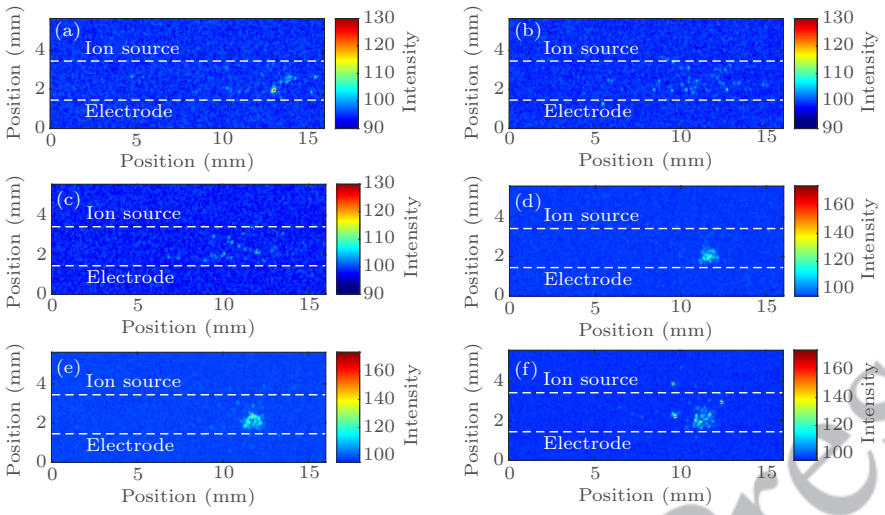


Fig. 6. Typical Ti atom luminescence images captured by high-speed camera: (a) $t = -60$ ns, (b) $t = -40$ ns, (c) $t = -20$ ns, (d) $t = 0$ ns, (e) $t = 20$ ns, (f) $t = 40$ ns.

During breakdown, Ti atoms also display localized luminescence near the electrode surface, with temporal evolution similar to that of H atoms. Nevertheless, the brightness is markedly lower than that of H atoms at comparable timescales.

This difference is likely to stem from Ti atom production requiring evaporation of electrode material. The local electrode surface temperature (Ti melting point ≈ 1940 K) significantly exceeds that for H atom release (≈ 620 K).[25,26] Thus, H atom release is more readily facilitated by the impact of Cu^+ ions on the electrode surface.

3.3. Analysis of ion-beam-induced vacuum breakdown with time-resolved spectroscopy

To obtain more precise information on particle composition during breakdown, a spectrometer was incorporated ahead of the high-speed camera. The spectrometer utilized a 300 lines/mm grating, with acquisition centered at 498 nm and 656 nm. The resulting spectrally dispersed images captured by the high-speed camera are shown in Figs. 7 and 8, with an exposure time and interval of 200 ns.

Figures 7 and 8 demonstrate that spectral lines associated with neutral Ti atoms (Ti I, 490–510 nm) and singly ionized Ti ions (Ti II, 440–460 nm) are virtually absent prior to breakdown. Following breakdown, the emission from Ti ions becomes pronounced, indicating that significant Ti ionization occurs primarily during the breakdown event itself, probably due to ablation and evaporation of electrode material. The minimal Ti-related emission before breakdown suggests negligible electrode evaporation prior to the event. Therefore, it can be concluded that titanium plays an insignificant role in the initial micro-discharge and the ignition of the breakdown.

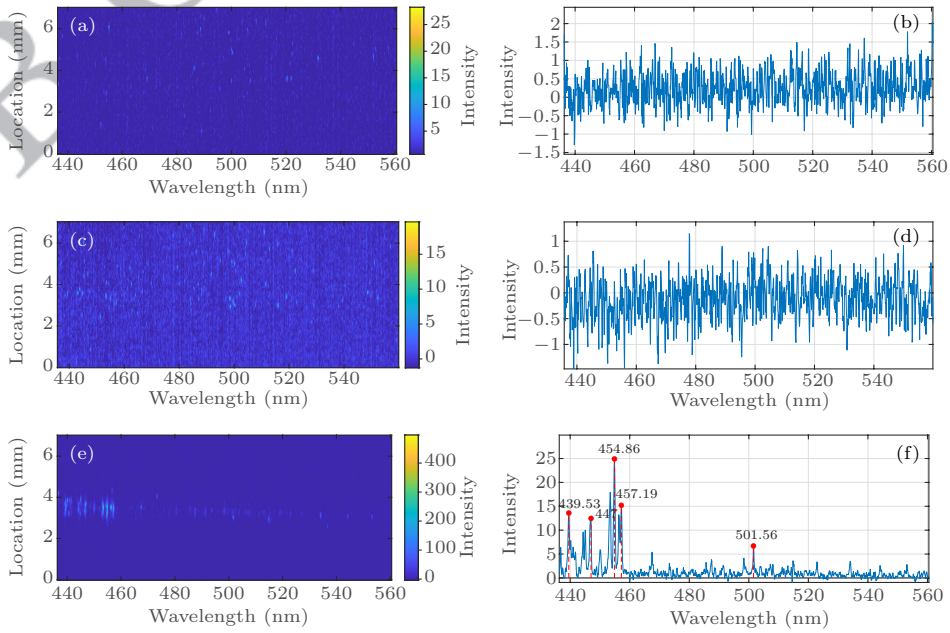


Fig. 7. Emission spectra of the breakdown (central wavelength 498 nm). Left, 2D spectra: (a) $t = -410$ ns, (c) $t = -210$ ns, (e) $t = -10$ ns. Right, line spectra: (b) $t = -410$ ns, (d) $t = -210$ ns, (f) $t = -10$ ns.

CPB Online In-Press

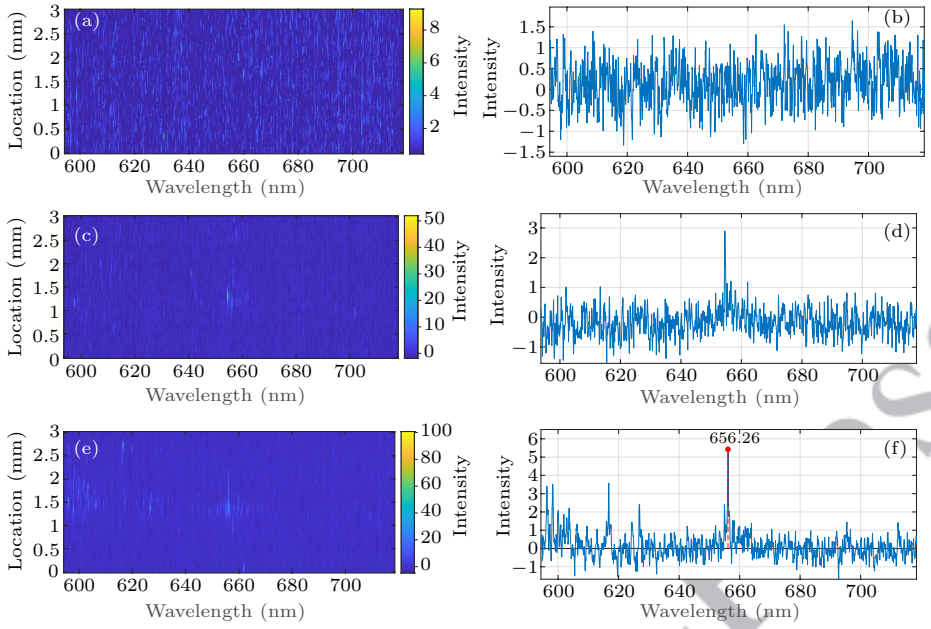


Fig. 8. Emission spectra of the breakdown (central wavelength 656 nm). Left, 2D spectra: (a) $t = -380$ ns, (c) $t = -180$ ns, (e) $t = 20$ ns. Right, line spectra: (b) $t = -380$ ns, (d) $t = -180$ ns, (f) $t = 20$ ns.

In contrast, the Hα emission line (H I, 656 nm) is present both before and after breakdown, consistent with the results of Fig. 5. This confirms that the desorption of H atoms from the electrode, induced by ion bombardment, is the critical factor initiating the cathode-mediated breakdown process under ion beam bombardment.

4. Discussion

In the physical process depicted in Fig. 9, bombardment of the hydrogen-containing electrode by the ion beam may generate H atom desorption, Ti atom sputtering, and secondary electron emission. Comprehensive analysis using ICCDs, high-speed cameras, and spectrometers reveals that high-energy Cu^+ ion bombardment of hydrogen-containing electrodes induces two distinct physical phenomena.

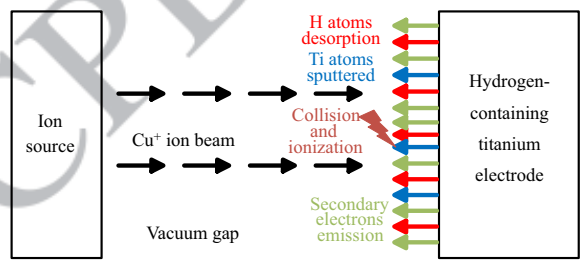


Fig. 9. Physical mechanism of bombardment of a hydrogen-containing electrode with a Cu^+ ion beam.

Under non-breakdown conditions, luminescence is distributed uniformly across the acceleration gap, with spectral analysis identifying near-ion-source emission as Cu atom de-excitation from source discharge. The Cu atom density decreases by orders of magnitude due to spatial diffusion from the ion source interior to the acceleration gap, resulting in weak luminescence confined near the source outlet. Near the electrode, luminescence is dominated by H atom de-excitation with minor contributions from Ti atoms as localized heating releases hydrogen (≈ 620 K[26]) below titanium evaporation thresholds (> 1000 K), while gap luminescence originates from H atoms rapidly propagating across the gap after electrode release.

Conversely, when bombardment induces breakdown, imaging techniques show no penetrating plasma channels in the gaps, indicating that the breakdown induced by ion beam bombardment on the electrode does not form an arc discharge. Spectroscopic analysis detects massive release of neutral particles from the electrode (predominantly H/Ti). Combined with the plasma motion analysis (i.e., due to significantly lower drift velocities compared with ions), the rate of neutral particles leaving the electrode surface is obviously lower than the rate of neutral particles released by ion bombardment. This imbalance leads to the accumulation of neutral particles near the electrode surface, which eventually forms a local high-density neutral particle region. Concurrent keV ion bombardment of the electrode will also generate secondary electron emission, which will be accelerated by the sheath near the electrode. Some of the electrons will collide with high-density neutral particles, ionizing them to produce new secondary electrons and positive ions. The new electrons further ionize the neutral particles, while the positive ions bombard the electrode under the action of an electric field to further release or evaporate additional neutrals (H/Ti). This cycle eventually leads to electrode surface ablation and electron avalanche. Ultimately, a large number of electrons migrate toward the ion source, inducing gap breakdown.

CPB Online In-Press

5. Conclusion

We constructed a high-voltage testing platform incorporating plasma emission spectroscopy to study the vacuum breakdown phenomenon induced by bombarding a hydrogen-containing titanium electrode with a Cu^+ ion beam at an acceleration voltage of 10 kV. Temporal and spatial luminescence and emission spectra images were obtained by ICCD, high-speed camera and spectrometer. Through temporal analysis of the continuous evolution in H/Ti atomic emission distributions and characteristic spectral profiles during pre- and post-vacuum breakdown phases, the following conclusions are derived.

(I) Irradiation of the surface by Cu^+ ion beams induces sputtering and desorption of significant hydrogen into the vacuum interelectrode gap. Neutral particles travel significantly slower than ions, causing accumulation near the electrode with the duration of ion beam bombardment. The resultant high-density neutral particle region near the electrode surface will significantly enhance the collision probability between it and the secondary electrons emitted by the electrode surface, leading to atomic excitation and subsequent radiative de-excitation, that is, significant luminescence near the electrode surface.

(II) Neutral atom accumulation beyond a critical threshold intensifies collisions with secondary electrons, which ionize to produce a large number of electrons and ions. This initiates an electron avalanche process that forms localized "micro-discharges", manifested as discrete luminescent clusters at the electrode interface — indicative of breakdown inception. The micro-discharges generate dense near-electrode plasma. Upon reaching critical neutral density thresholds, ionization of H/Ti neutrals produces both ions and new secondary electrons. The latter undergo field-driven acceleration, sustaining the ionization avalanche, while positive ions bombard the electrode surface to enhance thermal loading and neutral desorption. This self-sustaining feedback loop culminates in surface ablation. Ultimately, propagation of the electron flux toward the ion source initiates interelectrode breakdown.

Our work provides novel experimental insights into the physical processes of ion beam bombardment on electrodes, specifically through high-speed imaging of H and Ti atom luminescence dynamics. This approach offers a unique empirical foundation for understanding mechanisms such as micro-discharge formation, which has not been extensively documented in prior studies. This study elucidates fundamental physical processes governing electrode bombardment by an ion beam, establishing a mechanistic basis for further understanding.

Acknowledgements

Project supported by the Presidential Foundation of China Academy of Engineering Physics (Grant Nos. YZJJZQ2022016 and YZJJPY2025015) and the National Natural Science Foundation of China (Grant No. 52207177).

References

[1] Alpert D, Lee D A, Lyman E M and Tomaschke H E 1964 *J. Vac. Sci. Technol.* **1** 35
[2] Miller H C 2023 *IEEE Trans. Plasma Sci.* **51** 1585
[3] Wuensch W 2018 28th *ISDEIV*, September 23–28, 2018, Greifswald, Germany, p. 747
[4] Becker E W and Klingelhöfer R 1966 *Plasma Phys. Control. Fusion* **8** 413
[5] Gröbner O and Calder R S 1973 *IEEE Trans. Nucl. Sci.* **20** 760
[6] Erlandsson R 1980 *Appl. Surf. Sci.* **6** 473
[7] Baird S, Bosser J, Broere J, Carli C, Chanel M, Hill C, Ley R, Lombardi A, Maccaferri R, Maury S, Meshkov I, Möhl D, Molinari G, Mulder H, Syresin E, Tanke E, Tranqueille G, Varenne F and Vretenar M 1997 *Nucl. Instr. and Meth. in Phys. Res. A* **391** 17
[8] Zhang S Y and Ahrens L A 1998 6th *EPAC*, June 22–26, 1998, Stockholm, Sweden, p. 2149
[9] Spiller P 2010 *Proc. of HB*2010, September 26–October 1, 2010, Morschach, Switzerland, p. 34
[10] Meng J, Yang W S, Luo C, Xie W J, Chai Z, Li C C, Jiao J Q, Wan Y P, Liu J L, Lin X J, Ma X L, Zhu X R, Zhang X P and Wei N F 2021 *Chin. J. Vac. Sci. Technol.* **41** 826
[11] Li P, Yuan Y J, Yang J C, Li M, Kang X C, Ding J J, Luo C, Mao R S, Zhao T C, Chai Z, Zheng W H, Dong Z Q, Wang Y M and Yin Y 2019 *Nucl. Instr. and Meth. in Phys. Res. A* **920** 14
[12] Li P, Bozyk L, Dong Z Q, Spiller P, Li M, Yang J C, Yuan Y J, Luo C, Xie W J and Zheng W H 2019 *Vacuum* **163** 15
[13] Winters H F and Sigmund P 1974 *J. Appl. Phys.* **45** 4760
[14] Taglauer E, Beitat U, Marin G and Heiland W 1976 *J. Nucl. Mater.* **63** 193
[15] Taglauer E and Heiland W 1976 *Appl. Phys.* **9** 261
[16] Bourne H C, Cloud R W and Trump J G 1955 *J. Appl. Phys.* **26** 596
[17] Brainard J P and Riedel A A 1976 *J. Appl. Phys.* **47** 2911
[18] Zalucki Z and Kutzner J 1985 *IEEE Trans. Plasma Sci.* **13** 315
[19] Zhang X E, Zhang T P, Li D T and Li X 2022 *J. Phys.: Conf. Ser.* **2201** 012002
[20] Liu H, Zhang L, Liu W, Liu Y, Qi C and Zhang G 2024 *ICOPS*, June 22–26, 2024, Beijing, China
[21] Xu A, Jin D Z, Wang Y J and Tan X H 2020 *IEEE Trans. Plasma Sci.* **48** 888
[22] Methling R, Gortschakow S, Lisnyak M V, Franke S, Khakpour A, Popov S A, Batrakov A V, Uhrlandt D and Weltmann K D 2015 *IEEE Trans. Plasma Sci.* **43** 2303
[23] Khakpour A, Methling R, Uhrlandt D, Franke S, Gortschakow S, Popov S A, Batrakov A and Weltmann K D 2017 *J. Phys. D: Appl. Phys.* **50** 185203
[24] Khakpour A, Methling R, Franke S, Gortschakow S and Uhrlandt D 2018 *J. Appl. Phys.* **124** 243301
[25] Ma M W, Wang L, Tang B H, Lyu P, Xiang W, Wang Y and Tan X H 2018 *Int. J. Hydrog. Energy* **43** 1577
[26] Ma M W, Liang L, Wang L, Wang Y, Cheng Y L, Tang B H, Xiang W and Tan X H 2015 *Int. J. Hydrog. Energy* **40** 8926

CPB Online In Press